Tropical Journal of Pharmaceutical Research June 2026; 25 (6): 853-863
**ISSN:** 1596-5996 (print); 1596-9827 (electronic)

Available online at http://www.tjpr.org
**https://dx.doi.org/10.4314/tjpr.v25i6.11**

**Original Research Article**

# Pharmacognostic assessments and phytochemical mapping of ribwort plantain tissues: Integrated findings from ED-XRF, NMR and hyphenated chromatographic analyses

**Hasan Alauldeen Khalaf[1,2]*, Ibrahim S Abbas[1], Vahid Reza Askari[3,4,5]**

*[1]Department of Pharmacognosy and Medicinal Plants, College of Pharmacy, Mustansiriyah University, [2]Department of Pharmacognosy and Medicinal Plants, College of Pharmacy, Al-Bayan University, Baghdad, Iraq, [3]Patient Safety Research Center, Clinical Research Institute, [4]Transplant Research Center, Clinical Research Institute, Mashhad University of Medical Sciences, [5]Clinical Research Development Unit, Imam Reza Hospital, Faculty of Medicine, Mashhad University of Medical Sciences, Mashhad, Iran*

**For correspondence:* ***Email:*** *hasan.alaa@albayan.edu.iq;* ***Tel:*** *+9647706094491*

*Sent for review: 24 March 2026* *Revised accepted: 20 May 2026*

## Abstract

***Purpose:*** *To conduct a phytochemical mapping of ribwort plantain organs, with emphasis on organ-specific distribution of important bioactive compounds.*
***Methods:*** *Pharmacognostical and phytochemical characteristics of the plant parts were profiled using preliminary phytochemical screening, Energy Dispersive X-ray Fluorescence (ED-XRF), Gas Chromatography – Mass Spectrometry (GC-MS), Thin Layer Chromatography (TLC), High Performance Thin Layer Chromatography (HPTLC), Liquid Chromatography – Mass Spectrometry (LC-MS) and Nuclear Magnetic Resonance (NMR).*
***Results:*** *Preliminary test and GC-MS analysis of the plant revealed various phytochemical constituents of the plant parts. The ED-XRF findings revealed a high calcium level with the absence of toxic heavy elements (Pb, Cd, As). The LC-ESI-MS detected isolated phytochemicals as Na+ adducts, while NMR elucidated their structures.*
***Conclusion:*** *The study revealed isolated accumulation of active metabolites, with flowers and roots demonstrating higher levels of catalpol and aucubin, respectively, while seeds showed the lowest concentration of acteoside.*

***Keywords:*** *β-sitosterol, Iridoids, LC-ESI-MS, Plantago lanceolata, Verbascoside*



**Tropical Journal of Pharmaceutical Research is indexed by Scopus, Chemical Abstracts, Embase, Index Copernicus, EBSCO, African Index Medicus, JournalSeek, Directory of Open Access Journals (DOAJ), African Journal Online, Bioline International, Open-J-Gate and Pharmacy Abstracts**

## INTRODUCTION

*Plantago lanceolata* L. (Plantaginaceae family), commonly known as ribwort plantain (RP), has been studied for many years and is enshrined in traditional pharmacopoeias throughout Europe [1]. Aerial parts of RP are used as treatment for upper respiratory tract conditions, such as chronic bronchitis, asthma and common cold due to its demulcent and expectorant effect [2]. The various biological activities exhibited by RP are due to a vast array of phytochemical constituents [3]. The plant contains phenylethanoid glycosides (acteoside), flavonoids (luteolin, apigenin), mucilages and tannins. However, key bioactive compounds

include iridoid glycosides (aucubin and catalpol), which are monoterpenoidic compounds and significant chemotaxonomical markers of Plantago genus [4]. Current pharmacological studies have validated many of the traditional uses of RP. The iridoids have potent hepatoprotective and neuroprotective properties [5,6]. However, the presence of mucilages and flavonoids accounts for the immunomodulatory and antioxidative effect, while phytosterols and phenylethanoids exhibit anti-inflammatory effect [7]. These constituents exert a synergistic effect that inhibits pro-inflammatory pathways while improving tissue regeneration, providing a strong therapeutic rationale for their continued investigation [8]. Notwithstanding, there are limited details on the comparative chemical distribution across the aerial and underground parts of the plant. This study conducted a preliminary qualitative phytochemical screening on the leaves, flowers, roots and seeds of RP, and a metabolic mapping of different fingerprints of the plant parts. By identifying and isolating different phytochemicals across these distinct parts, this study provided a scientific foundation for the part-specific use of RP in nutraceutical and pharmaceutical products.

## EXPERIMENTAL

### Plant preparation

The leaves, roots, seeds and flowers (L, R, S and F) of RP were collected and authenticated by a taxonomist, with voucher specimens deposited in the national herbarium of Iraq (no. 52739). Each part was carefully separated, cleaned, dried, powdered, sieved, and stored in tightly sealed containers at 5 $^{o}$C prior to extraction [9,10].

### Plant extraction

Extraction was accomplished using Soxhlet's apparatus. The powdered plant part (15 g) was extracted with chloroform for 6 h. The residual marc of each part was dried, extracted with methanol for 6 h, and concentrated using vacuum evaporator at 40 $^{o}$C, and subjected to standard preliminary phytochemical investigations [11].

### Micronutrients analysis

Micronutrients of RP leaves powder were analysed using energy-dispersive X-ray fluorescence (ED-XRF; Bruker CTX spectrometer) under standard operating conditions (X-ray tube voltage fixed at 50 kV, current set at 225 µA to enhance count rate, spectrum obtained at 100 sec, dead time of the detector (DT %) was retained at 30 % to confirm signal linearity).

### Gas chromatography-mass spectrometric analysis (GC-MS)

Profiling of volatile compounds obtained from the chloroform extracts was accomplished using a Restek Rxi-35Sil MS column (30 m length × 0.25 mm diameter x 0.25 mm thickness; Shimadzu GC-2010 Pro). The temperature started at 50 $^{o}$C for 2 min, followed by a stepwise increment at 15 $^{o}$C/min up to 150 $^{o}$C, sustained for 5 min, then ramped at 20 $^{o}$C/min to 270 $^{o}$C with final holding for 5 min. Helium (99.99 %) was used at a flow rate of 1 mL/min.

### Thin-layer chromatography (TLC) analysis

Separation of phytochemicals was carried out using CAMAG TLC automatic sampler 4 on a precoated silica gel 60 F 254 plate. Each extract (1 g) was dissolved in methanol (10 mL) and applied as a band (10 mm length) with a 3 µL injection volume. The test was performed in triplicate for iridoids. The iridoids designated as S1a, S1b, and S1c were separated using chloroform: methanol: trifluoroacetic acid (0.25 M) in ammonia (60:50:15 v/v/v), butanol: distilled water (DW): acetic acid (AA; 40:10:10 v/v/v) and n-propanol: ethylacetate: AA (85:35:5 v/v/v), respectively. Acteoside was separated using ethylacetate: formic acid: AA: DW (85:5:5:5 v/v/v/v), while S3 mobile phase (toluene: ethylacetate: ethanol (8:2:1 v/v/v)) was used to separate β-sitosterol. The phytochemicals were isolated from the extracts using preparative TLC (20×20 cm, 0.5 mm), comparing with a reference standard [12].

### Structural elucidation analysis

Structures of the phytochemicals were elucidated using an LC-ESI-MS and $^{1}$H and $^{13}$C NMR systems. Separation of the methanol extract was performed on a Kromasil 100-5 C18 column (150 mm×4.6 mm, 5 µm) using a gradient elution composed of 0.1 % formic acid in water (solvent A) and 0.1 % formic acid in acetonitrile (solvent B) at a flow rate of 0.25 mL/min. Mass fragmentation was carried out using a Shimadzu UFLC-AB Sciex 3200 QTRAP Mass Spectrometer, which ran in positive electrospray ionization mode (+ESI), and a capillary voltage of 4.5 kV. Spectra of $^{1}$HNMR were recorded at 400 MHz (100 MHz for $^{13}$CNMR) on a 400 MHz Bruker NMR spectrometer utilizing deuterated water ($D_2O$) and chloroform ($CDCl_3$) as solvents for glycosides and phytosterol, respectively.

## RESULTS

### Phytochemical content

Preliminary phytochemical screening of RP revealed that the plant parts have irregular, yet diverse secondary metabolite content. The leaves have been identified as the most chemically active part, followed by the flowers, having the highest iridoid glycoside content and the most diverse secondary metabolites (Table 1).

### Micronutrients profile

The ED-XRF analysis of RP leaves powder revealed the presence of chlorine (34.39 %), calcium (31.27 %), and potassium (24.89 %). Essential trace elements, including iron (2.54 %), zinc (0.11 %), and manganese (0.14 %), were also identified. Toxic heavy metals such as Pb, Cd, and As were not detected (Table 2).

### Gas chromatography – mass spectroscopy (GC-MS) profile

The plant showed a rich fatty acid profile including linoleic, linolenic, myristic and palmitic acids, and ethyl linoleate in addition to different types of terpenoids and phytosterols (Table 3).

### Thin-layer chromatography

The HPTLC-densitometric analysis revealed the presence of iridoid glycosides in RP. The methanol flower extract (MFE) had the highest level of catalpol compared to other parts. Levels of aucubin varied across the extracts, with the methanol root extract (MRE) having the highest concentration. Comparative study of iridoids between plant extracts showed low variability with relative standard deviation (RSD %; 2.24 - 6.83 %; Table 4; Figure 1). These iridoid glycosides have an $R_f$ value of 0.36 - 0.63, with S1 mobile phases (Table 5).

### Thin-layer chromatogram of Acteoside

On the other hand, the thin-layer chromatogram of acteoside demonstrated that phenylpropanoid glycosides were below the detectable level in MSE, though a low level was also observed in MRE. The TLC and HPTLC results revealed that the highest level of acteoside was found in the MFE, with a mean peak area about twice that of MLE. In contrast to phenylethanoids, iridoids are not visible under UV light at 254 and 366 nm (Figure 2).

**Table 1**: Preliminary phytochemical screening of RP

| Test | Methanol Extract | | | | Chloroform Extract | | | |
|---|---|---|---|---|---|---|---|---|
| Trim-Hill test for iridoid glycosides | L | F | S | R | L | F | S | R |
| $FeCl_3$ test for Tannins | + | + | + | + | - | - | - | - |
| Alcoholic KOH for flavonoids | + | + | + | + | + | + | - | - |
| Dragendorff test for alkaloids | + | + | + | - | - | - | - | - |
| Salkowski test for phytosterols | - | - | - | - | + | + | + | + |
| Froth-forming test for saponins | + | + | + | + | - | - | - | - |
| Chemical test for terpenes | + | - | - | - | + | + | + | + |

**Table 2:** Micronutrients of RP

| Element | Result±SD (%) | Intensity |
|---|---|---|
| Cl | 34.385±0.266 | 6.1797 |
| Ca | 31.266±0.215 | 8.1332 |
| K | 24.891±0.213 | 5.1728 |
| S | 5.480±0.100 | 0.9283 |
| Fe | 2.535±0.022 | 4.9012 |
| Sr | 0.527±0.007 | 5.2841 |
| Ti | 0.244±0.026 | 0.1142 |
| Br | 0.238±0.007 | 1.8757 |
| Cu | 0.161±0.009 | 0.5788 |
| Mn | 0.142±0.013 | 0.1981 |
| Zn | 0.111±0.007 | 0.4755 |
| Rb | 0.019±0.005 | 0.1722 |

**Table 3:** GC-MS profile of RP

| Compound | RT (min) | SI (%) | Leaf (area %) | Root (area %) | Flower (area %) | Seed (area %) |
|---|---|---|---|---|---|---|
| 1,2-xylene | 4.595 | 98 | - | 12.61 | - | - |
| 2-Hexyldecanol (Exxal 16) | 18.495 | 89 | 2.85 | - | - | - |
| 3-methylene-1-1-vinyl-1-cyclopentane | 4.050 | 92 | - | 31.31 | - | - |
| 6-octadecanoic acid methyl ester | 18.608 | 91 | - | - | 2.62 | - |
| D-Limonene | 6.940 | | - | - | 0.71 | - |
| Elaidic Acid (9-Octadecenoic acid) methyl ester | 18.485 | 94 | - | - | 4.64 | - |
| Ethyl linoleate | 21.085 | 91 | - | - | 16.94 | - |
| Heptacosanal | 26.435 | 94 | 4.6 | - | 2.58 | - |
| Hexahydrofarnesyl acetone | 20.135 | 92 | - | - | 2.79 | - |
| Hexatriacontane | 23.660 | 95 | 6.12 | - | - | 5.7 |
| Lauric acid | 15.415 | 93 | - | - | 4.76 | - |
| Linoleic acid | 20.38 | 90 | 8.82 | 2.16 | - | - |
| Linolenic acid | 20.55 | 95 | 4.28 | - | - | - |
| Maleic acid bis(2-ethylhexyl) ester | 20.305 | 81 | - | - | - | 4.3 |
| Methyl cinnamate | 14.170 | 95 | - | - | 1.51 | - |
| Methyl linoleate | 18.815 | 95 | - | - | 36.06 | - |
| Methyl melissate | 16.955 | 83 | - | - | 2.31 | - |
| Myristic acid | 17.850 | 95 | - | - | - | 10.8 |
| Nonacosanal | 25.415 | 94 | 4.6 | 2.58 | - | - |
| Palmitic acid | 18.445 | 95 | 16.83 | 4.73 | 10.92 | 14.62 |
| Phthalic acid, bis(ethyl hexyl) ester | 24.045 | 95 | 5.4 | 2.02 | - | 4.22 |
| Phytyl tetradecanoate | 27.075 | 94 | - | 8.63 | - | - |
| Sabinene | 7.100 | | - | - | 0.45 | - |
| Spathulenol | 18.630 | 84 | 0.83 | - | - | - |
| Stearic acid | 20.31 | 91 | 17.44 | - | - | 10.8 |
| Stigmasterol acetate | 28.550 | 72 | 2.94 | - | - | - |
| Tetracontane | 25.150 | 94 | - | - | - | - |
| Tetracosane | 28.325 | 94 | 3.08 | - | - | 4.14 |
| β-Phellandrene | 7.100 | | - | - | 0.45 | - |
| β-Sitosterol acetate | 29.755 | 89 | - | 3.51 | - | - |

Retention time (RT), Similarity index (SI)

**Table 4:** Peak areas of iridoids from HPTLC

| Compound | Peak Area ± SD (RSD %) | | | |
|---|---|---|---|---|
| | ***MLE*** | ***MSE*** | ***MRE*** | ***MFE*** |
| Catalpol | 2216.11±110.92(5.01) | 7588.24±225.71(2.97) | 829.02±49.41(5.96) | 40463.62±1695.73(4.19) |
| Aucubin | 3880.82±264.31(6.81) | 3170.45±216.42(6.83) | 5564.40±232.03(4.17) | 2549.90±123.02(4.82) |
| Catalpol/Aucubin | 0.57 | 2.39 | 0.15 | 15.86 |

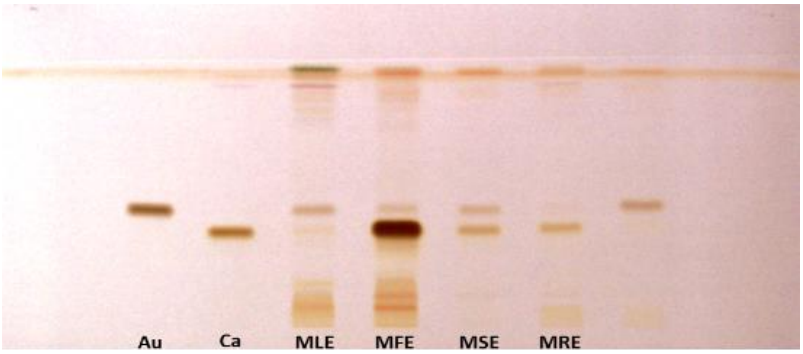


**Figure 1:** Thin-layer chromatogram of iridoids

**Table 5:** $R_f$ Values of Iridoids across Different Samples

| Solvent | Au (sd) | Ca (sd) | MLE | MSE | MRE | MFE |
|---|---|---|---|---|---|---|
| S1a | 0.45 | 0.36 | 0.44,0.37 | 0.44,0.37 | 0.46,0.38 | 0.45,0.38 |
| S1b | 0.53 | 0.48 | 0.51,0.47 | 0.53,0.48 | 0.53,NA | NA,0.49 |
| S1c | 0.63 | 0.53 | 0.63,0.54 | 0.64,0.54 | 0.62,NA | NA,0.52 |

Au = aucubin, Ca = catalpol. Their $R_f$ values are separated by a comma (Au, Ca)

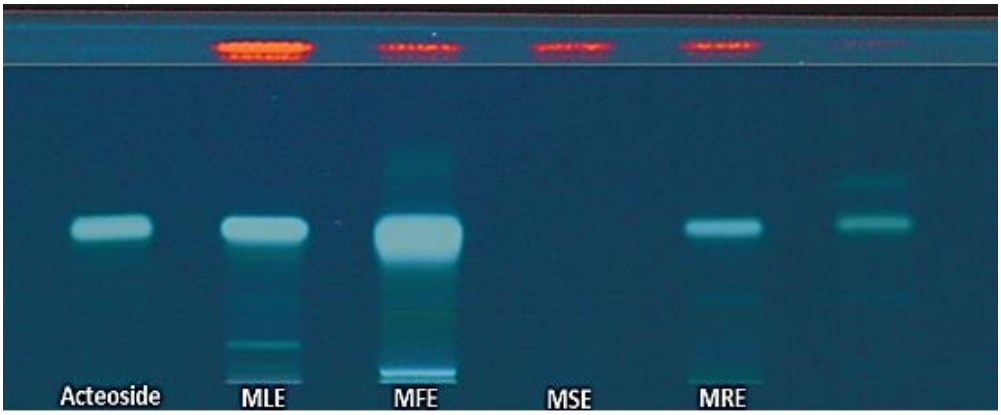


**Figure 2:** TLC chromatogram of acteoside

### Qualitative analysis of chloroform extracts

Qualitative analysis of chloroform extract (CE) of RP by TLC/HPTLC revealed the presence of β-sitosterol in all plant parts (CLE, CSE, CRE and CFE). Identification was validated by a distinctive spot that co-migrated exactly beside the β-sitosterol standard with $R_f$ values of 0.46 - 0.67 (Figure 3).

### Liquid chromatography – mass spectrometry (LC-MS) of aucubin and catalpol

The LC-MS analysis in +ESI mode showed retention times of 6.93 - 7.17 and 6.69 - 7.04 min for aucubin and catalpol, respectively, displaying the distinctive polar features of iridoid glycosides. The base peaks were represented by the $Na^+$ adducts $[M+Na]^+$ at m/z of 369.1 and 385.2 for aucubin and catalpol, respectively. Intense fragments of aucubin were observed at 121.3 m/z, 131.3 m/z and 149.2 m/z, while catalpol showed distinctive peaks at 137.1 m/z, 147.2 m/z, 165.2 m/z, and 183.2 m/z (Figure 4).

### Liquid chromatography – mass spectrometry (LC-MS) of acteosides

The standard acteoside and acteoside in all the methanol extracts showed a retention time of

13.37 - 13.52 min. The LC-MS result showed different adducts of acteoside ($H^+$, $Na^+$, $K^+$, and $NH_4^+$), with sodium adduct being the most prominent (Figure 5). The LC-MS examination of β-sitosterol effectively captured its ionization behavior through production of two distinct adducts, $[M+H]^+$ at 415.3 m/z and $[M+Na]^+$ at 437.1 m/z, and β-sitosterol structure was elucidated at retention time of 23.039 - 23.139 min (Figure 5).

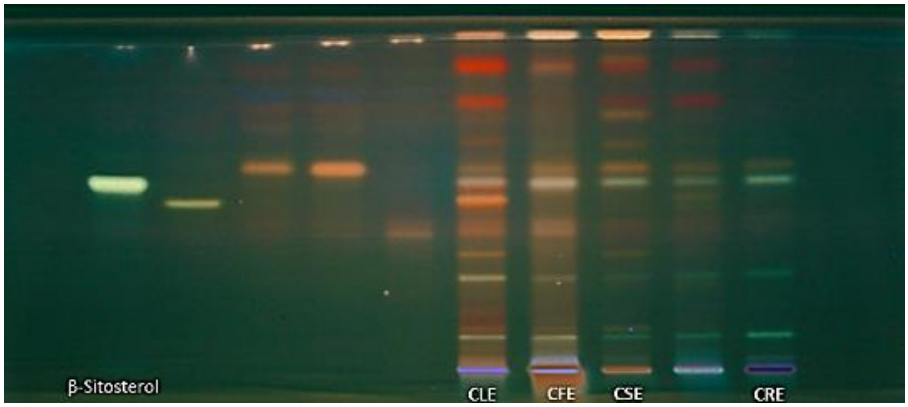


**Figure 3:** TLC chromatogram of β-sitosterol

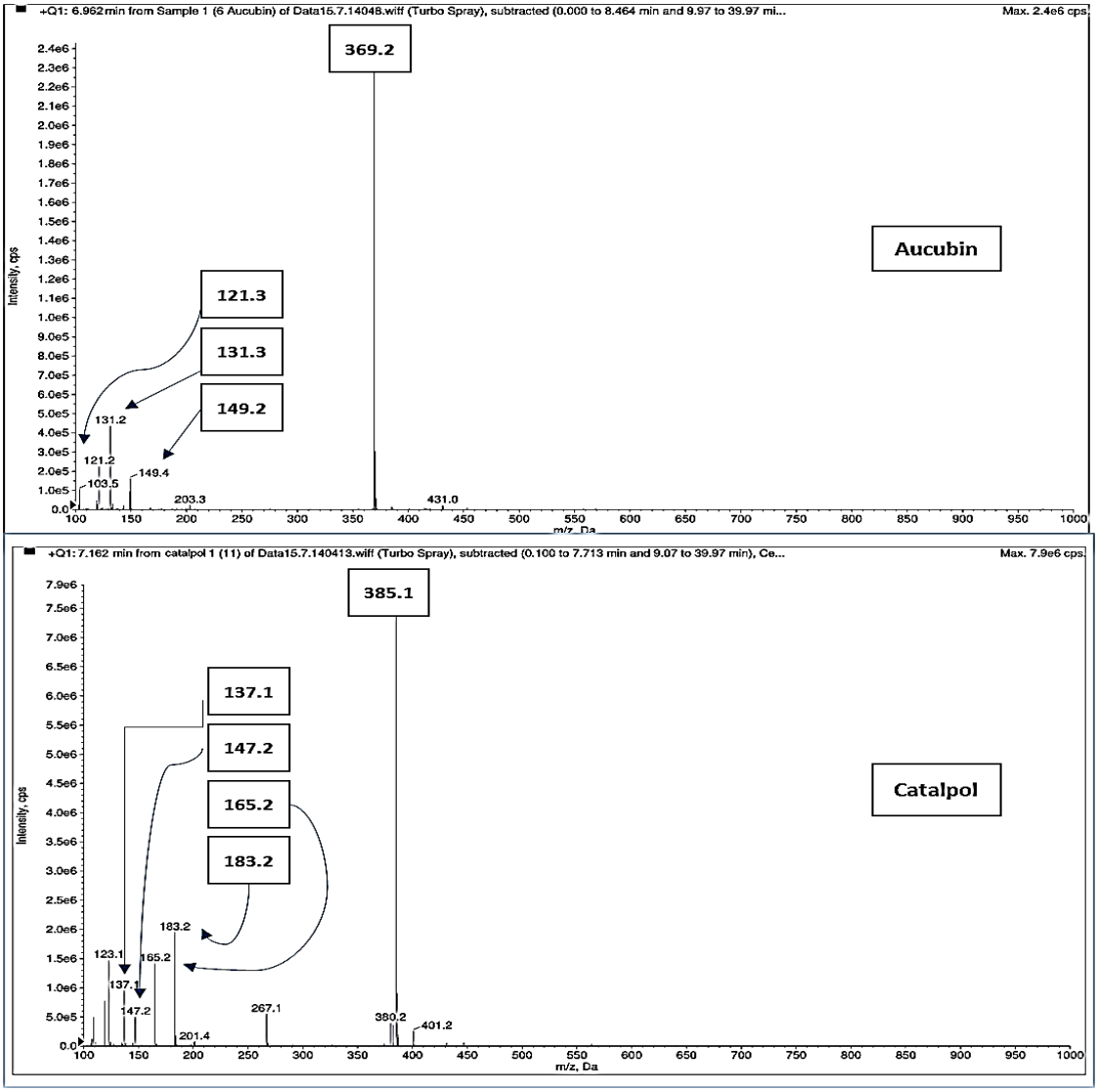


**Figure 4:** Mass fragmentation of iridoids

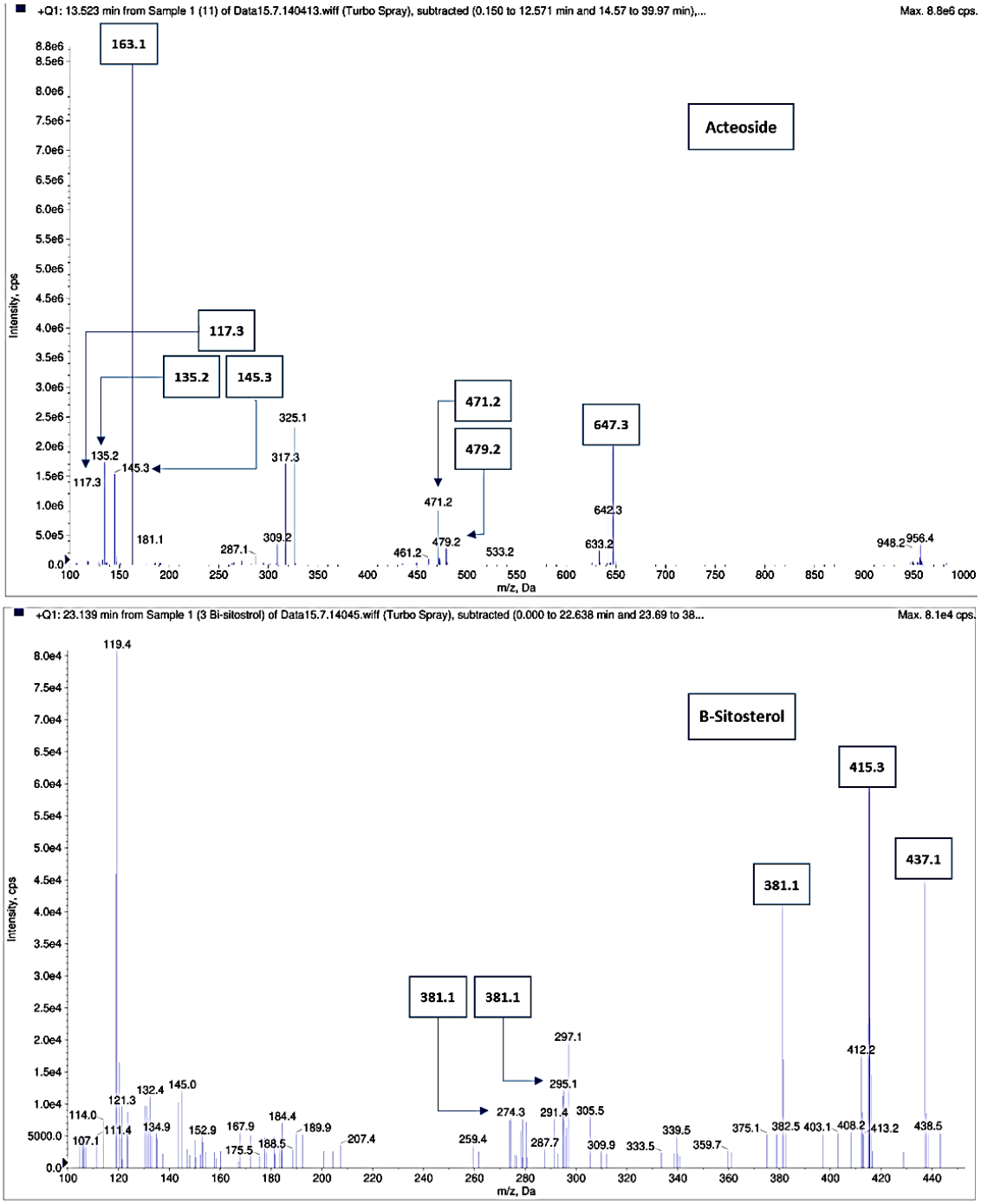


**Figure 5:** Mass fragmentation of acteoside and β-sitosterol

## Nuclear magnetic resonance (NMR) imaging

**Compound 1** (Figure 6 A) was purified as a white crystal, LC-+ESI-MS 369 m/z $[M+Na]^+$ (calculated as $C_{15}H_{22}O_9$): $^1$HNMR (400 MHz, $D_2O$): δ 6.24 (1H, d, J= 6.0 Hz, H-3), 5.80 (1H, br s, H-7), 5.23 (1H, d, J= 5.2 Hz, H-1) 5.08–5.04 (1H, m, H-4), 4.74 (1H, d, J= 8.0 Hz, H-1'), 4.49 (1H, br s, H-6), 4.32–4.21 (2H, m, H-10a,b), 3.86 (1H, m, H-6'b), 3.66 (1H, m, H-6'a), 3.50-3.26 (4H, m, H-2',3',4',5'), 3.12–3.09 (1H, m, H-9), 2.74 (1H, m, H-5); $^{13}$CNMR (100 MHz, $D_2O$): δ 146.7 (C-8), 139.4 (C-3), 128.3 (C-7), 105.1 (C-4), 95.2 (C-1), 80.4 (C-6), 59.4 (C-10), 46.2 (C-5), 42.19 (C-9), 98.7 (C-1'), 76.1 (C-3'), 75.5 (C-5'), 72.6 (C-2'), 69.4 (C-4'), and 60.5 (C-6').

**Compound 2** (Figure 6 B) was purified as a white crystal, LC-+ESI-MS 385 m/z $[M+Na]^+$ (calculated as $C_{15}H_{22}O_{10}$: $^1$HNMR (400 MHz, $D_2O$): δ 6.36 (1H, dd, J= 6 Hz, H-3), 5.12 (1H, m, H-4), 5.06 (1H, dd, J=9.6 Hz, H-1), 4.25 (1H, dd,

J= 13.2 Hz, H-10a), 4.04 (1H, d, J= 8 Hz, H-10b), 3.87 (1H, d, J=12.4 Hz, H-6), 3.59 (1H, s, H-7), 4.84 (1H, d, J= 8 Hz, H-1'), 3.73 (1H, d, J= 13.2 Hz, H-6'b), (1H, m, H-6'a), 3.34-3.51 3.73 (1H, m, H-2',3',4',5'), 2.59-2.63 (1H, m, H-9), 2.25-2.30 (1H, m, H-5); $^{13}$CNMR (100 MHz, $D_2O$): δ 140.4 (C-3), 103.0 (C-4), 94.6 (C-1), 77.5 (C-6), 62.1 (C-8), 60.6 (C-7), 60.1 (C-10), 41.6 (C-9), 37.2 (C-5), 98.5 (C-1'), 77.5 (C-5'), 76.1 (C-3'), 75.5 (C-2'), 72.7 (C-4'), and 65.7 (C-6').

**Compound 3** (Figure 6 C) was purified as a yellow powder, LC-+ESI-MS 646 m/z $[M+Na]^+$ (calculated as $C_{29}H_{36}O_{15}$): $^1$HNMR (400 MHz, $D_2O$): δ 7.65 (1H, d, J = 15.6 Hz, H-7'), 7.16 (1H, S, H-2'), 7.10 (1H, d, J = 8.4 Hz, H-6'), 6.90 (1H, d, J= 8.0 Hz, H-5'), 6.82 (2H, d, J = 6.8 Hz, H-2, H-5), 6.72 (1H, d, J= 8.0 Hz, H-6), 6.36 (1H, d, J= 16 Hz, H-8'), 5.07 (1H, br s, H-1'''), 4.92 (1H, t, J= 9.2 Hz, H-4') 4.44 (1H, d, J= 8.0 Hz, H-1''), 3.78-3.89 (2H, m, H-2'', H-2'''), 3.58-3.70 (5H, m, H-3'', H-4'', H-5'', H-8), 3.43-3.53 (3H, m, H-6'', H-4'''), 3.41 (1H, t, J= 8.6 Hz, H-3'''), 3.39 (3H, t, J= 9.6 Hz, H-4'''), 2.79 (2H, t, J= 6.4 Hz, H-7); $^{13}$CNMR (100 MHz, DMSO): δ 166.2 (C-9'), 148.9 (C-4'), 146.0 (C-7'), 145.9 (C-3), 145.4 (C-3'), 143.9 (C-4), 129.5 (C-1), 125.9 (C-1'), 121.9 (C-6'), 120.0 (C-6), 116.7 (C-2), 116.2 (C-5'), 115.9 (C-5), 115.2 (C-2'), 113.9 (C-8'), 102.7 (C-1''), 101.7 (C-1'''), 79.5 (C-3''), 74.9 (C-5''), 72.0 (C-5'''), 70.9 (C-3'''), 70.78 (C-4'''), 70.74 (C-4''), 69.6 (C-8), 69.2 (C-2''), 61.2 (C-6''), 35.5 (C-7), and 18.6 (C-6''').

**Compound 4** (Figure 6 D) was purified as a white crystal, LC-+ESI-MS 437.1 m/z $[M+Na]^+$ (calculated for $C_{29}H_{50}O$): $^1$HNMR (400 MHz, $CDCl_3$): δ 5.37 (1H, m, H-6), 3.54 (1H, m, H-3), 1.01 (3H, m, H-19), 0.94 (3H, d, H-21), 0.80-0.90 (9H, m, H-26, 27 and 29), 0.68 (3H, s, H-18), 1.05-2.29 (29H, steroid overlap); $^{13}$CNMR (100 MHz, $CDCl_3$): δ 140.7 (C-5), 121.7 (C-6), 71.8 (C-3), 56.7 (C-14), 56.0 (C-17), 50.8 (C-9), 45.8 (C-24), 42.3 (C-13), 42.2 (C-4), 39.8 (C-12), 37.2 (C-1), 36.5 (C-10), 36.1 (C-20), 33.9 (C-22), 31.92 (C-7), 31.90 (C-8), 31.6 (C-2), 29.1 (C-25), 28.3 (C-16), 26.0 (C-23), 24.3 (C-15), 23.1 (C-28), 21.1 (C-11), 19.9 (C-27), 19.4 (C-19), 19.0 (C-26), 18.8 (C-21), 12.0 (C-29), and 11.8 (C-18).

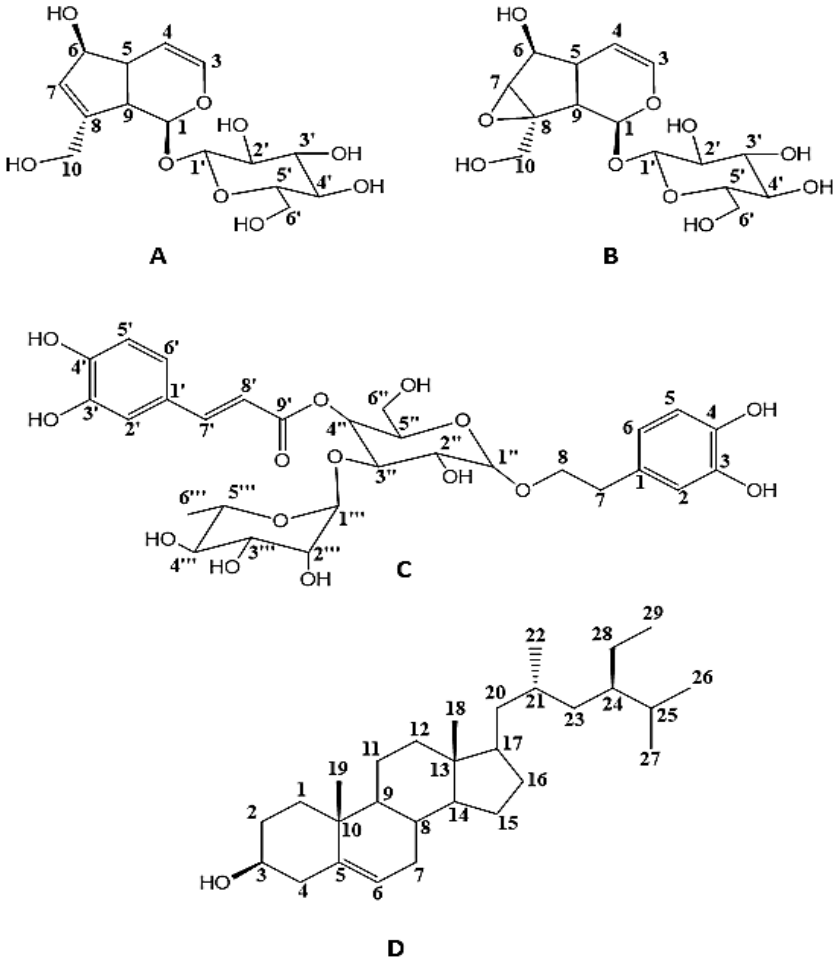


**Figure 6:** Structures of isolated phytochemicals from RP

## DISCUSSION

Phytochemical profiling of RP in this study was achieved with an integrated analytical approach, utilizing a combination of chromatographic and spectroscopic techniques to ensure high-confidence metabolite identification. Preliminary phytochemical screening of different plant parts showed a unique metabolic pattern, marked by undetected alkaloids with a preponderance of iridoid glycosides consistent with previous study [13]. Results from the micronutrient analysis by ED-XRF confirmed that the RP leaves powder is safe from toxic heavy metals. For example, the absence of lead (Pb), cadmium (Cd), arsenic (As), and mercury (Hg) is a clear indication that the product met the safety limit as recommended by the WHO/FDA regulations on herbal products [14]. The plant is rich in calcium and potassium, consistent with findings from a previous study [15].

The plant parts exhibited complex GC-MS patterns. The prominent occurrence of free fatty acids in RP was in tandem with earlier metabolomic analysis performed on the plant [16]. This study revealed that the chloroform leaf extract has a lipophilic profile, which is in line with other investigations that found palmitic acid and 9-octadecenoic acid as major compounds [17,18]. Compared to recent GC-MS analysis of the lipophilic extract, the phytochemical profile of RP chloroform leaf extract was characterized by stearic acid, palmitic acid, and a group of long-chain alkanes. Current study, however, showed a more complicated profile of terpenoids and sterol esters and much greater relative abundance of important free fatty acids [19]. Comparative phytochemical profiling of RP by TLC and HPTLC demonstrates a highly part-specific distribution of bioactive metabolites. The catalpol/aucubin ratio was highest in MFE, whereas the highest recorded abundance of aucubin was observed in MRE. While acteoside peaked in MLE and MFE, it was not detected in MSE. Conversely, β-sitosterol was ubiquitously distributed across all parts, and preliminary phytochemical screening and HPTLC analysis confirmed the ubiquitous presence of iridoid glycosides in the parts studied. The base peaks of iridoids were represented by $Na^+$ adducts, confirming the incidence of $Na^+$-associated pseudomolecular ions typical for these iridoids [20]. Aucubin and catalpol each showed two distinctive peaks at different retention times, and both peaks showed a similar mass spectrum. This finding is in agreement with the anomerization or mutarotation (interconversion) phenomenon, especially in the presence of a protic solvent [21]. The intense fragments of aucubin were observed at 121.3, 131.3 and 149.2 m/z, while catalpol showed distinctive peaks at 137.1, 147.2, 165.2, and 183.2 m/z, which aligned with an earlier study [22]. Fragmentation spectrum attained in +ESI mode exposed a diagnostic triad of ions at 167.2 m/z (unstable), 149.2, and 131.3 m/z for aucubin, and 183.2, 165.2, and 147.2 m/z for catalpol, which was produced subsequently by deglycosylation and stepwise dehydration of the protonated aglycone $[M+H]^+$. Also, another signal that differentiated these closely related iridoids was 121.2 m/z and 103.1 m/z for aucubin, which resulted from the neutral loss of CO (28 Da) from 149.2 and 131.3 Da, respectively, while catalpol showed a fragment peak at 137.1 m/z produced by CO loss from 165.2 Da. A recent study found the peak transition as 149.2 m/z to 131.3 m/z for aucubin, which served as a consistent mass spectrometric indicator to positively identify and confirm the presence of aucubin in the plant extract [23].

Base peak in the mass spectrum of acteoside was permanently 163 m/z, represented by the dehydrated form of protonated caffeic acid [caffeic acid+H-$H_2O$]$^+$. This was observed in addition to other common peaks of protonated caffeic acid at 145.3 m/z, 135.2 m/z, and 117.3 m/z, which are essential substructure features of phenylpropanoid glycosides that resulted from loss of $2H_2O$ (36 Da), $H_2O$ + CO (46 Da), and $2H_2O$ + CO (64 Da), respectively [24]. The detected peak at 325.2 m/z is a common feature in +ESI mode, indicating the presence of acteoside, which is tentatively $[M+H-HT]^+$ adduct, followed by a specific rearrangement to generate this characteristic signal [25]. Comparison of tandem mass spectra of proton and sodium adducts revealed a coherent and striking fragmentation pattern of β-sitosterol. Three parallel pathways of fragmentation of these adduct ions at 274.3 m/z for $[M+H]^+$ and 295.1 m/z for $\{M+Na\}^+$ due to loss of the side chain at C17, and a signature of steroidal nucleus with a signal at 119.3 m/z represented the base peak. Natural loss of a methyl group produced fragments at 259.4 and 279.6 m/z for proton and sodiated adducts, respectively. Furthermore, the congruent loss of $CH_4$ and $H_2O$ generated ions at 381.1 m/z for the proton adduct and 403.1 m/z for the sodiated adduct, pinpointing important diagnostic peaks of β-sitosterol [26]. The NMR spectra for iridoid glycosides displayed diagnostic signals for the iridoid skeleton, with the most distinctive difference being the presence of an epoxide proton (H-7) and the corresponding $^{13}C$ signals (C-7 and C-8) in catalpol, while aucubin was characterized by the presence of an allylic (H-6) near δ 4.49 and

vinylic substituents (H-7) at δ 5.80, as noted in previous studies [27]. The phenylethanoid glycoside (acteoside) was confirmed by a complex set of aromatic signals in the δ 6.5–7.5 range representing hydroxytyrosol and caffeoyl moieties, alongside characteristic trans-vinylic doublets (H-7 and H-8) of caffeic acid residue with a distinctive H-7 proton, which is deshielded at δ 7.6. Moreover, acteoside exhibited a characteristic $^{13}C$ signal represented by the carbonyl carbon that resonated at δ 166.2 in tandem with a previous study [28]. Also, isolation of β-sitosterol was confirmed by distinctive sterol markers, including vinylic proton H-6 at δ 5.37 and hydroxylated methine H-3 at δ 3.54, with $^{13}C$ resonances at δ 140.7 (C-5), 121.8 (C-6), and 71.7 (C-3) [29].

## CONCLUSION

Four phytochemicals (aucubin, catalpol, acteoside, and β-sitosterol) have been isolated, with flowers and roots of *Ribwort plantain* (RP) demonstrating higher levels of catalpol and aucubin, respectively, while seeds showed the lowest concentration of acteoside.

## DECLARATIONS

### Acknowledgement/Funding

The authors are thankful to the College of Pharmacy, Mustansiriyah University, Baghdad, Iraq; Mashhad University of Medical Sciences, Mashhad, Iran, for support, and Al-Bayan University, Baghdad, Iraq, for sponsorship.

### Ethical approval

Not applicable.

### Use of Artificial intelligence/Large language models

The authors confirm that AI-based tools were used solely for language editing and manuscript polishing purposes (e.g., grammar, phrasing, and clarity). No AI tools were used to generate content, interpret data, or influence study design, results, or conclusions. All intellectual contributions, study analyses, and interpretations reported in the manuscript are the original work of the authors.

### Availability of data and materials

The datasets used and/or analyzed during the current study are available from the corresponding author on reasonable request.

### Conflict of interest

No conflict of interest is associated with this work.

### Contribution of authors

We declare that this work was done by the author(s) named in this article, and all liabilities pertaining to claims relating to the content of this article will be borne by the authors.

## REFERENCES

1. *Tröber F, Pol M, Krauss M, Schmidtke K. Impact of ribwort plantain (Plantago lanceolata L.) and mixtures with red clover (Trifolium pratense L.) as a precrop of winter wheat (Triticum aestivum L.) on nitrous oxide and methane emissions. Agric Ecosyst Environ 2026; 397: 110088*
2. *Stojanović S, Karsunky M, Damnjanović I, Najdanović J, Savić V, Najman S. Influence of vitamin C and ribwort plantain extract addition to the propolis extract on the viability of fibroblasts in cell culture in vitro. Acta Med Medianae 2025; 64(2): 56-63*
3. *Işık M, Sümer E. Phytochemical compositions and bioactive properties of Plantago lanceolata L.: anti-oxidant, anti-diabetic, and anti-cholinergic potentials. J Oleo Sci 2025; 74(8): 721-728*
4. *Rahamouz-Haghighi S, Bagheri K, Sharafi A. Investigating a simple and sensitive high-performance liquid chromatography method for simultaneous determination of apigenin, catalpol, and gallic acid contents in Plantago lanceolata L. and Plantago major L. Pharm Biomed Res 2023; 9(4): 297-310*
5. *Li W, Ma X, Mei Y, Peng C, Feng Z. Aucubin inhibits liver cancer via HMGB1-mediated inactivation of the PI3K/AKT/mTOR signaling pathway. Recent Pat Anticancer Drug Discov 2026; 21: e15748928420661*
6. *Li W, Zhou X. Catalpol: a promising natural neuroprotective agent for neurologic disorders. Acta Mater Med 2025; 4(3): 413-436*
7. *Wu Y, Wang X, Wang C, Ma X. Medicine-food homologous Plantago L. in gastrointestinal health and disease: a review. Mol Nutr Food Res 2025; 69(16): e70100.*
8. *Laanet PR, Bragina O, Jõul P, Vaher M. Plantago major and Plantago lanceolata exhibit antioxidant and Borrelia burgdorferi inhibiting activities. Int J Mol Sci 2024; 25(13): 7112*
9. *Ahmed SF, Ahmed FN. Antibacterial activity of celery (Apium graveolens) extract against urinary tract infections: antimicrobial activity of Apium graveolens extract. Al-Mustansiriyah J Pharm Sci 2025; 25(5): 1004-1015*
10. *Khalaf HAA, Mahdi MF, Abaas IS. Preliminary phytochemical and GC-MS analysis of chemical*

constituents of Iraqi Plantago lanceolata L. Al-Mustansiriyah J Pharm Sci 2018; 18(2): 114-121

11. Khalaf HA, Abbas IS, Tawfeeq AA, Mahdi MF. Determination, isolation, and identification of aucubin and verbascoside in the leaves of Iraqi Plantago lanceolata L. using different detection methods. Int J Pharm Pharm Sci 2018; 11(2): 74-80
12. Dhanapal SS, Balachandran P, Ranganathan S. HPTLC and FTIR studies on iridoid glycoside (negundoside) isolated from ethanol leaf extracts of Vitex negundo Linn. Afr J Biomed Res 2024; 27(3): 432-443
13. Tariq S, Mehmood A. Pharmacognosy and phytochemical screening of Plantago major L. and Plantago lanceolata L. from Rawalakot, Azad Jammu and Kashmir. Kashmir J Sci 2022; 1(1): 1-11
14. World Health Organization. WHO guidelines for assessing the quality of herbal medicines with reference to contaminants and residues. 2007: 1-188
15. Guil-Guerrero JL. Nutritional composition of Plantago species (P. major L., P. lanceolata L., and P. media L.). Ecol Food Nutr 2001; 40(5): 481-495
16. Rahamouz-Haghighi S, Sharafi A. Biocompatibility, cytotoxicity and phytochemical analysis of Plantago lanceolata L. aerial extracts: in vitro and in vivo study. Era J Med Res 2024; 11(1): 8-24
17. Bajer T, Janda V, Bajerova P, Kremr D, Eisner A, Ventura K. Chemical composition of essential oils from Plantago lanceolata L. leaves extracted by hydrodistillation. J Food Sci Technol 2016; 53(3): 1576-1584. doi:10.1007/s13197-015-2083-x
18. Rahamouz-Haghighi S, Bagheri K, Mohsen-Pour N, Sharafi A. In vitro evaluation of cytotoxicity and antibacterial activities of ribwort plantain (Plantago lanceolata L.) root fractions and phytochemical analysis by gas chromatography-mass spectrometry. Arch Razi Inst. 2022 Dec 31;77(6):2131-2143. doi: 10.22092/ARI.2022.358045.2143.
19. Rahamouz-Haghighi S, Bagheri K, Sharafi A. Antibacterial activities and chemical compounds of Plantago lanceolata (ribwort plantain) and Plantago major (broadleaf plantain) leaf extracts. Pharm Biomed Res 2023; 9(3): 183-200
20. Akbari S, Abdurahman NH, Fayaz F, Noory V. Iridoids of fenugreek (Trigonella foenum-graecum L.) seed extract detected via LC-QTOF-MS analysis. Future Foods 2021; 4: 100067
21. Serse F, Trespi S, Paloni M, Salvalaglio M, Mazzotti M. Solvent-mediated mechanism and kinetics of glucose mutarotation from enhanced sampling simulations. J Chem Phys 2025; 163(16): 164504
22. Ivanova B. Stochastic dynamics mass spectrometric quantification and 3D molecular structural analysis of tricyclic antidepressant in marine dissolved organic matter. Environ Geochem Health 2025; 47(6): 211
23. Upadyshev M, Ivanova B, Motyleva S. Mass spectrometric identification of metabolites after magnetic-pulse treatment of infected Pyrus communis L. microplants. Int J Mol Sci 2023; 24(23): 16776
24. Zhong L, Lu M, Fang H, Li C, Qu H, Ding G. Secondary metabolites from Rehmannia glutinosa protect mitochondrial function in LPS-injured endothelial cells. Pharmaceuticals 2025; 18(8): 1125
25. Obied HK, Bedgood DR Jr, Prenzler PD, Robards K. Chemical screening of olive biophenol extracts by hyphenated liquid chromatography. Anal Chim Acta 2007; 603(2): 176-189
26. Islam MJ, Rahman HMA, Jahan N, Mostafa MG, Akter B. Isolation, structural characterization and molecular docking of β-sitosterol from Trewia polycarpa root bark: a potential source of bioactive compounds. Discov Chem 2025; 2(1): 156
27. Jadav G, Dodia S, Kher P, Shah P, Kataria D, Khunt RC, et al. Aucubin as a natural therapeutic and optical material: a computational study on its structural, spectroscopic, and photonic properties. Int J Quantum Chem 2025; 125(10): e70054
28. Paniagua-Vega D, Huerta-Heredia AA, Sánchez-Otero MG, Waksman-Minsky N, Lucio-Gutiérrez JR, Saucedo AL. NMR and chemometric analysis of verbascoside and isoverbascoside produced in Tecoma stans in vitro cultures. Magn Reson Chem 2025; 63(8): 593-603
29. Tristyaningrum NA, Herlina T, Kurnia D. β-sitosterol from Piper crocatum: a dual-action antifungal and antibacterial agent for oral infections. Trends Sci 2025; 22(10): 10420